Original Article

Microstructural evaluation of Inconel 625 weld cladding deposited by the GMAW and GMAW with rotating electrode processes

Jeferson Frederico Monteiro Costa [1]
Jorge Carlos Ferreira Jorge [1]*
Luís Felipe Guimarães de Souza [1]
Matheus Campolina Mendes [1]
Humberto Nogueira Farneze [1]
Hiron Akira Yamada Magalhães [1]

Abstract

The microstructure of the Inconel 625 single layer weld cladding deposited by the conventional GMAW and GMAW with rotating electrode (GMAW-RE) processes on carbon steel is investigated. Metallographic characterization was performed on samples removed transversally to the weld deposit by optical and scanning electron microscopy equipped with energy dispersive spectrometry to evaluate the secondary phases. The results showed that the GMAW-RE process provided a more homogeneous penetration and a lower dilution rate than the GMAW process. As a consequence, a reduced Fe content and a refined austenitic microstructure with a lower amount of secondary phases were observed, factors that contribute greatly to better overlay performance. This superior performance indicates that the GMAW-RE process has the potential to be an advantageous alternative for Inconel 625 weld claddings.

Keywords: Nickel alloy 625; GMAW-RE process; Weld metal; Welding; Secondary phases.

Avaliação microestrutural de revestimentos depositados com Inconel 625 pelos processos GMAW e GMAW com eletrodo rotativo

Resumo

Este trabalho realiza uma análise comparativa da microestrutura de revestimentos com Inconel 625 depositados em camada única pelos processos GMAW convencional e GMAW com eletrodo rotativo (GMAW-RE) sobre aço carbono. A caracterização metalográfica foi realizada em amostras removidas transversalmente ao depósito de solda por microscopia ótica e eletrônica de varredura equipada com espectrometria de energia dispersiva para avaliação de fases secundárias. Os resultados mostraram que o processo GMAW-RE permitiu a deposição com penetração mais homogênea e menor taxa de diluição que o processo GMAW. Como consequência, foi observado um teor do elemento Fe reduzido e uma microestrutura austenítica refinada com menor fração de fases secundárias, fatores que contribuem sobremaneira para um melhor desempenho do revestimento. Este melhor comportamento indica que o processo GMAW-RE tem potencial para ser uma alternativa vantajosa para soldagem de revestimento com Inconel 625.

Palavras-chave: Liga de níquel 625; Processo GMAW-RE; Metal de solda; Soldagem; Fases secundárias.

1 Introduction

Although high strength steels are extensively applied in the oil and gas industry, they are prone to corrosion due to the aggressive environments found in subsea conditions. As a consequence, a nobler alloy such as Inconel 625 is used due to its superior corrosion resistance [1]. However, the high cost of Inconel 625 sometimes limits the application in massive structures. To overcome this issue, Inconel 625 weld cladding deposited to protect the cheaper base material from corrosion is a feasible alternative widely observed in petroleum, naval, chemical, and nuclear industries [2-4].

Weld cladding can be produced by various processes, such as gas tungsten arc welding, shielded metal arc welding,

[1]*Centro Federal de Educação Tecnológica, Celso Suckow da Fonseca, Diretoria de Pesquisa e Pós-graduação, Rio de Janeiro, RJ, Brasil.*

**Corresponding author: jorgecfjorge@gmail.com*

gas metal arc welding (GMAW), and their variants. Particularly, the GMAW process is one of the most accepted processes due to its good quality, productivity, versatility, and robustness to allow application in complex geometries and different environments [4-6]. Its higher deposition rate contributes to reducing dilution by increasing arc efficiency and improving corrosion resistance [7]. At least two layers are usually necessary to reduce the dilution and attain the minimum thickness required of 3 mm of the corrosion-resistant layer with adequate chemical composition [8-13]. However, the application of conventional arc welding processes sometimes compromises the corrosion performance due to the high dilution of the base material [13]. Particularly, the diffusion of Fe into the clad is regarded as a critical issue and the maximum allowable Fe content is limited to 10% [8]. Although processes such as cold metal transfer [1,2,14,15], GMAW cold wire [5,11], electro slag [16,17], spin arc gas metal arc welding [18], and GTAW hot wire (GTAW-HW) [13,15,19-24] were developed to improve the quality without compromising productivity, they still can present limitation to replace the conventional processes.

The GTAW-HW is a widely used method for cladding critical parts of subsea equipment because it presents advantages such as high efficiency and good quality, associated moderate investment of equipment, and low running costs further boosting the widespread application of the hot wire pulsed TIG in surface modification [20-22,25]. Controversially, Babyak et al. [15] comment that this process produces aesthetic welds but low deposition rates and travel speeds increase the cost of production. It is also a comparatively high heat input process, meaning industrial cooling mechanisms within the torch head are needed to extend work efficiency. Although the GTAW-HW is the industry standard to clad pipes with corrosion resistant alloys (CRA) for the production of oil, where the risk of stress corrosion crack exists, Farias et al. [23], state that two layers of clad are still necessary to fulfill standard requirements for the Brazilian pre-salt oil and gas exploration [8] because these specifications cannot be met with a single clad layer. It is observed in Table 1, where it is worth noting that insufficient thicknesses of weld overlays are noted, although some processes can generate a single layer cladding with an acceptable low dilution ratio.

The Gas Metal Arc Welding Process with Rotating Electrode (GMAW-RE) is an advance of the GMAW process, where the wire rod is submitted to a rotating movement, with pre-specified rotation frequency and diameter [8], as shown in Figure 1b. The rotating movement provides weld beads deposited with lower penetration, lower dilution, and more homogeneous profile because they are more flat and shallow (Figure 2).

Although promising results with the rotating electrode are shown for narrow gap welding [29-31], this process is not well widespread yet and only one work studying a superaustenitic stainless steel weld overlay deposited by this process is available [18]. The authors [18] studied the influence of rotation frequency on the main geometric characteristics and microstructure and concluded that the GMAW-RE process has the potential to be an advantageous alternative for claddings because a lower dilution ratio is obtained.

Table 1. Dilution and thickness of single-layer weld overlays obtained by different processes [1,4,10,12,22,23,26-28]

Ref	Process	Thickness (mm)	Fe content (%)
1	CMT	2	4.1
	GTAW	2	12.6
4	GMAW (Ar25He)	3.5	13.6
	GMAW (Ar15CO_2)	3.0	26.9
10	SMAW	3.7	23.4
12	SMAW	3-4	22.0
	GMAW	3-3.5	13.0
	CMT	2.5-3	2-2.6
	GTAW-HW	3.0-3.5	6.6
	PAW	3.0-3.5	7.5
23	GTAW-HW	3.0	8.4
24	GTAW-HW	1.6	23.7
26	GMAW-CW	2.5	5.2
27	CMT	3.0	1.0
28	GTAW-HW	3.0-3.5	8.13

Where: CMT – Cold metal transfer; GTAW-HW – GTAW hot wire; PAW –Plasma arc welding; GMAW-CW – GMAW cold wire.

This work compares the weld bead geometric characteristics and microstructure of single layer Inconel 625 weld clads deposited by the conventional GMAW and GMAW-RE processes to evaluate the potential of the latter process as an alternative to produce weld overlay claddings with quality

2 Materials and methods

2.1 Materials

Samples with dimensions of 210×200×19 mm removed from API 5L X65 steel pipes were used as substrate and Inconel 625 wire of diameter 1.1mm of the class AWS A5.14 ER NiCrMo-3 [32] was used as filler metal in all experiments. Table 2 presents the chemical composition of the materials, as informed by the suppliers.

2.2 Welding procedure

A single layer with four welding passes was deposited by the GMAW and GMAW-RE processes to study the microstructure and the main geometric characteristics of the weld deposits, such as penetration, dilution, and geometry of the beads.

Welding was carried out in a flat position, with a preheat of 100 °C, the average current being 215 ampères, the average voltage 35 Volts, and the average welding speed 20 cm/min. A Miller welding power source model Millermatic 350P with pulsed current (synergic mode) was employed.

Table 2. Chemical composition of the materials informed by the suppliers (wt%)

Material	C	Si	Mn	Ni	Cr	Mo	Nb	Fe	Ti
Base metal	0.08	0.30	1.27	0.19	0.02	-	0.05	Bal.	0.02
Filler metal	0.015	0.01	0.01	65.20	21.58	8.79	3.61	0.19	0.16

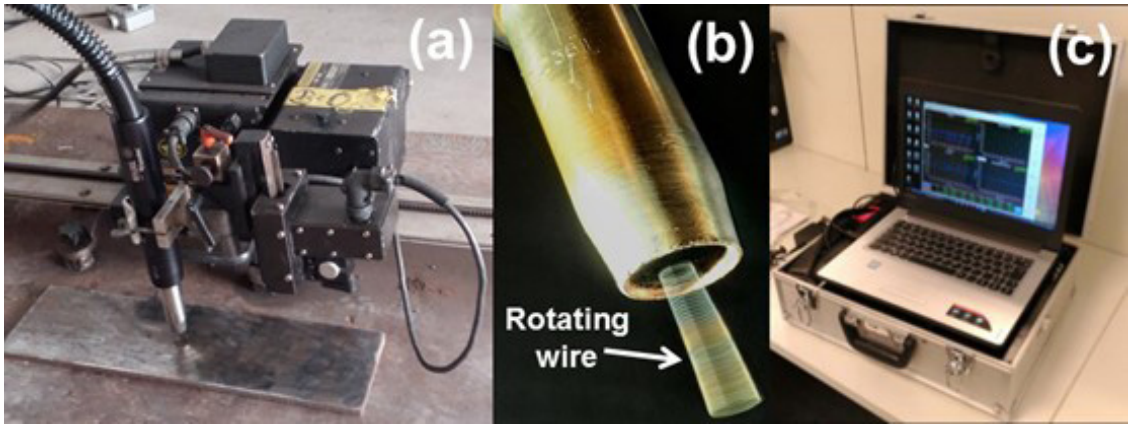

Figure 1. Details of the equipment used in welding. (a) Assembling for welding; (b) Welding torch showing the rotating wire; (c) Parameters monitoring device.

Ar-25%He with a flow rate of 25 L/min was applied as shielding gas. For the GMAW-RE process, the rotating frequency and rotating diameter of 1,500 rpm and 3 mm, respectively, were used, as suggested by other works [29-31]. All beads were deposited overlapping by 50% of the previous weld bead. The welding parameters were obtained from a portable welding parameter monitoring system, with an acquisition rate of 5 kHz (Figure 1c).

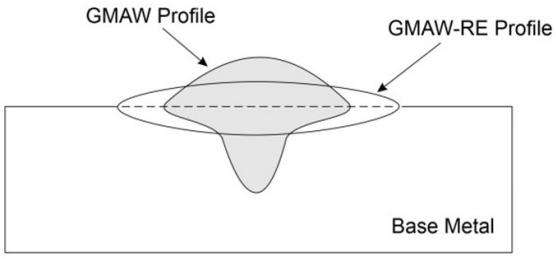

Figure 2. Effect of electrode rotation on weld bead profile.

2.3 Metallographic examination and microhardness tests

After welding, samples were transversely sectioned for metallographic examination and microhardness tests.

Metallographic examination by optical microscopy (OM) and scanning electron microscopy (SEM) with energy dispersive spectrometry (EDS) was carried out to clarify the microstructure at the positions related to the fusion line and at 3mm from the fusion line, the minimum thickness required [8].

The samples were prepared by conventional grinding and polishing procedure with diamond paste up to 0.25 µm. The etchants applied were 2% nital for the base metal and electrolytic oxalic acid (10%) for the deposited weld metal.

A semi-quantitative analysis of the elements appearing in the dendritic (D) and interdendritic (ID) regions and secondary phases in the weld metal was assessed by EDS. The volume fraction of secondary phases was investigated using the Image J software. For this analysis, ten different fields were observed with SEM and a nominal magnification of 1,000x at 3mm from the fusion line.

The values of dendrite arm spacing (DAS) were obtained by direct length readings on the optical microscope equipped with image analysis software.

The global dilution (D_G) was determined in the transverse cross-section by the ratio between the cross-sectional area of the melted substrate and the total cross-sectional area of the deposited overlay with the aid of the Image J software.

The local dilution ratio (D_L) was determined following Equation 1 based on the Fe content at 3mm from the fusion line.

$$D_L = (Cwm - Cfm)/(Cbm - Cfm) \quad (1)$$

Where: Cwm – Chemical composition of weld metal; Cfm – Chemical composition of filler metal; Cbm – Chemical composition of base metal.

Vickers microhardness ($HV_{0.5}$) tests were performed according to ASTM E 384 standard [33] at the same positions where the metallographic examination was conducted.

2.4 Chemical analysis

The chemical composition of the weld deposits was determined by optical emission spectroscopy at the top of the claddings.

3 Results

Figure 3 shows the macrographs of the weld deposits, where no evidence of porosities, cracks, or lack of fusion, and different penetration profiles are observed. The interface between the GMAW-RE weld deposit and the substrate is flatter and narrower than the GMAW weld deposit with a lower amount of base material melted. The thicknesses of the deposits are 5.1+/-0.3 mm and 3.6+/-0.3 mm for the GMAW-RE and GMAW processes, respectively. Equivalent values for the GMAW process were obtained by other authors [4]. A global dilution ratio of 9% is provided by the GMAW-RE process, while a value of 14% is observed for the GMAW process. This last result is usually obtained in the first layer of weld overlays deposited by the GMAW process [5,12,13,34,35].

These results agree with the chemical composition shown in Table 3, where a lower Fe content is observed for the GMAW-RE process. In addition, higher values of the main elements Ni, Cr, and Mo, are also obtained for this process, thus suggesting a better performance in comparison with the GMAW process.

Figure 4 shows details of the microstructure along with the fusion line where the following zones can be distinguished on cross-sections: weld metal, non-etched partially mixed zone (PMZ), and base metal. PMZs are macrosegregations that are intrinsic to dissimilar welds, whose chemical composition and mechanical properties differ from those

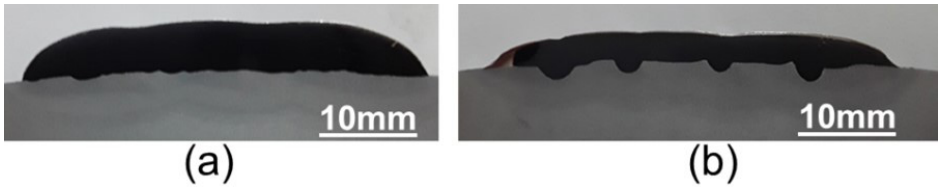

Figure 3. Macrographs of the weld overlays after etching with oxalic acid and nital 2% (OM). GMAW-RE; (b) GMAW.

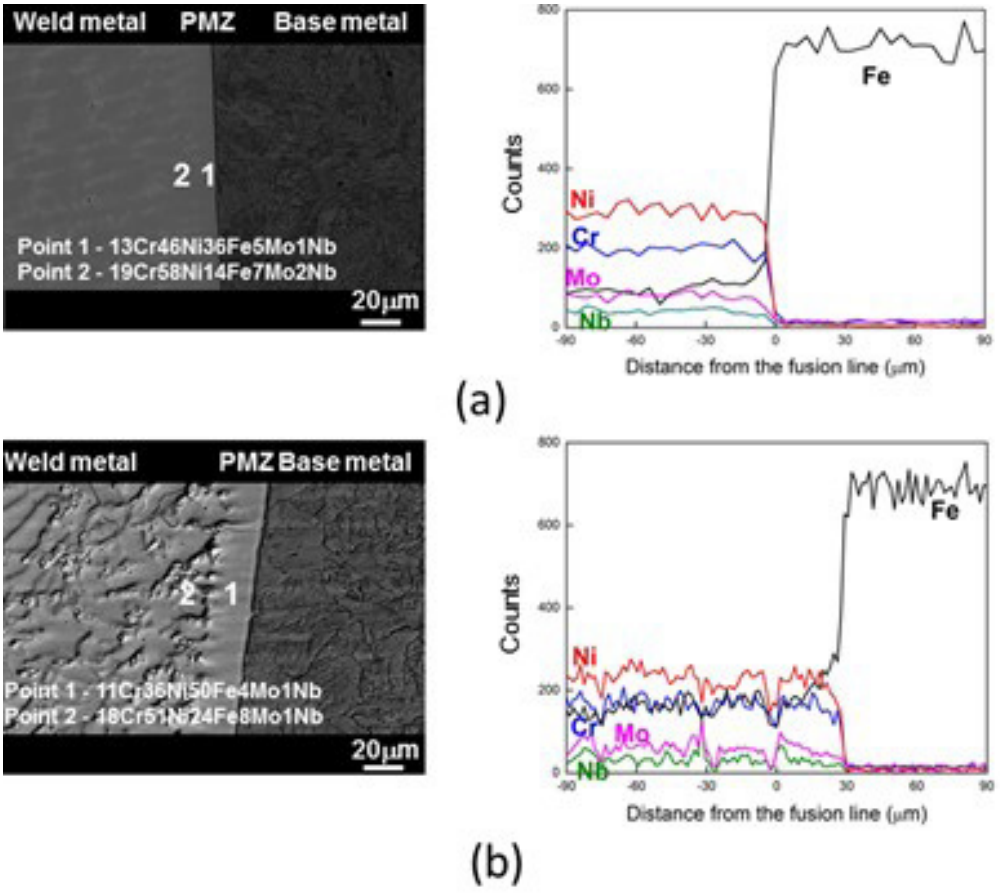

Figure 4. SEM images in the BSC mode and chemical composition profile obtained by EDS along the fusion line of the overlays. (a) GMAW-RE; (b) GMAW. Etchants: Oxalic acid and 2% nital.

Table 3. Chemical composition of the weld deposits obtained by optical emission spectroscopy at the top surface

Process	Element (weight, %)								
	C	Mn	Si	Ni	Cr	Mo	Cu	Nb	Fe
GMAW-RE	0.05	0.22	0.10	56.60	18.25	7.70	0.01	3.22	13.38
GMAW	0.05	0.34	0.10	51.60	16.33	6.87	0.01	2.85	21.44

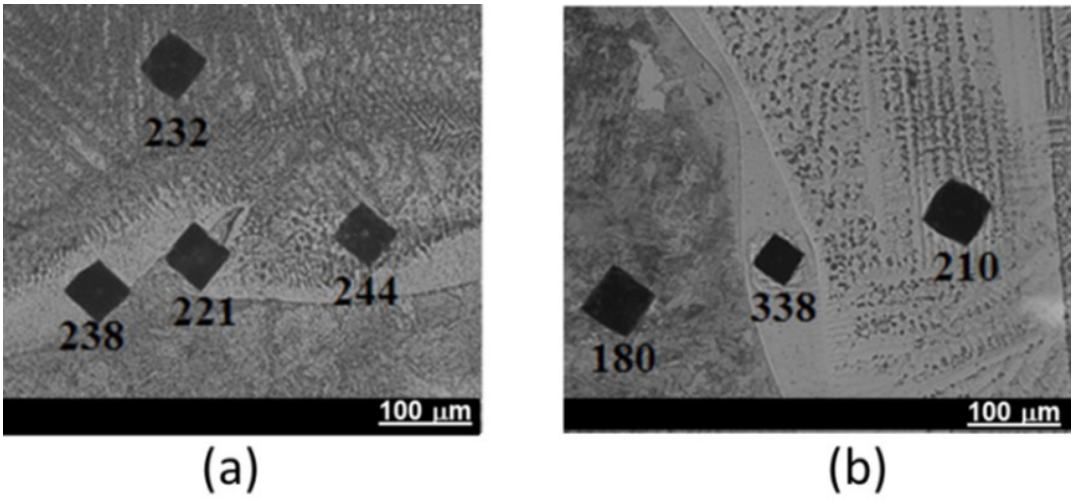

Figure 5. Microhardness values ($HV_{0.5}$) obtained at the fusion line. (a) GMAW-RE and (b) GMAW overlays.

of the weld and the substrate [5]. Also, the stabilization of the chemical composition is obtained for smaller distances from the fusion line, inducing that a low dilution ratio can be obtained closer to the fusion line, even for single layer weld overlays. In addition, the lower dilution contributed to avoiding the occurrence of hard microstructures close to the fusion line (Figure 5). These results agree with the low microhardness observed (Figure 6).

Figure 7 shows the microstructure of the coarse-grained region of the heat affected zone (CGHAZ). While bainite predominates for the GMAW-RE process, a mixture of ferrite, bainite, and martensite is observed for the GMAW process. The low microhardness results obtained (Figure 6) are attributed to the tempering promoted by multiple welding passes.

Regarding the microstructure of the deposited weld metal, an austenitic matrix with secondary phases in the interdendritic areas was observed (Figure 8). The values of primary and secondary dendrite arm spacing were 17+/-3 µm and 9+/-1 µm for the GMAW-RE deposit, and 17+/-3 µm and 9+/-2 µm for the GMAW process, indicating that no significant differences were observed. These values are equivalent to those obtained in other works [7,36-39].

The quantitative analysis of the secondary phases revealed a lower fraction of secondary phases obtained by the GMAW-RE process (1.6+/-1%) compared to the GMAW process (4.5+/-0.6%). Figure 9 shows a more detailed result of secondary phases obtained by the SEM/EDS technique. The irregularly shaped phase was identified as the Laves phase, because it presents eutectic-type morphology with a chemical composition containing high Nb content, approximately combining with $(Ni,Cr,Fe)_2(Nb,Mo,Si,Ti)$ type and showing a spectrum with a character well known. The square-shaped precipitates are rich in C and Nb and are classified as NbC-type MC primary carbides. The results are consistent with other works studying Inconel 625 weld metals [17,24,35,40-42].

4 Discussion

The literature states that the composition of materials and bead shape are the most influential parameters in improving mechanical and corrosion properties because they affect dilution, a major concern in claddings [3,43]. In this respect, Figure 3 shows the smoother penetration profile obtained by the GMAW-RE process because the rotation of the arc provides a heat distribution more homogeneous with a reduced flow in the vertical direction [44], thus promoting a broader temperature profile and wider heat distribution [45,46]. It prevents finger type penetration by dispersing the arc force over a wide area [47]. Consequently, the rotation of the arc also contributes to the slow cooling rate at the HAZ, inducing a less hardenable microstructure. It is also noted that equivalent dendrite arm spacings were obtained. Although an increased dendrite arm spacing is expected for slower cooling [7,42], sometimes no significant changes are noted for small differences in the heat input [37,42].

However, it is important to remember that the weld bead height is also crucial because the minimum thickness

required for claddings [8] must be attained with the lower volume of the deposited material to obtain good quality at an acceptable cost. In this respect, the GMAW-RE process showed an advantageous performance compared with the GMAW process for all these parameters. At last, it is also important to cite that the heat input used is higher than the other works. It is well known that the increase in heat input tends to increase the iron content due to greater dilution [13].

Figure 4 shows the region closest to the fusion boundary where neither grain boundaries nor cellular or dendritic growth are observed. It is named the planar growth zone formed in a planar way, according to the constitutional supercooling theory. It is noted that the planar region produced by the GMAW-RE process is narrower than that obtained by the GMAW process. For the GMAW-RE process, a steep transition and higher contents of Cr, Ni, and Mo than the GMAW process are observed (Figure 4), indicating that the dilution during welding was mitigated by the GMAW-RE process. The narrow planar growth region due to the insufficient mixture between dissimilar materials exhibits a sharp compositional gradient [28]. Studies performed by other researchers [5,12] indicate the planar solidification mode as the origin of a region dominated by a partially mixed zone (PMZ).

The occurrence of partially mixed zones (PMZ) is usual in Inconel 625 weld overlays, and fundamentals of macrosegregation have been detailed elsewhere [21,22,42,48]. Macrosegregation is usual in weld cladding due to the solute segregation during solidification leading to a composition gradient, and they are unavoidable because the time required for liquid diffusion is much too long during the GMAW process [44]. They are usually considered as an issue because they can cause hydrogen and stress-corrosion cracking since a thin zone containing a martensitic microstructure with high hardness can be formed [21,49]. It is more critical when substrates such as the AISI 8630 steel, typically used in subsea equipment, containing higher carbon contents are involved [21,22,50].

However, it can be minimized with the optimization of the welding parameters to control the cooling rate, and carbon dilution can promote a drastic reduction of partially diluted zones [45].

Although the literature registers that hard martensitic microstructures are expected in PMZs [11,40-42,49], the behavior observed for the GMAW-RE process was different (Figures 5 and 6). The occurrence of martensite was not verified and lower microhardness values were obtained, even when discontinuities similar to peninsulas were considered. For the GMAW process, higher microhardness values are observed solely when a beach-type discontinuity is found. As per the chemical composition estimated by EDS point analysis, in agreement with the Schaeffler diagram (Figure 10), the weld metal is fully austenitic, even for an unusually high dilution obtained in the PMZ of the GMAW process. The occurrence of a mixture of martensite + austenite is expected solely for the beach-type discontinuity (Figure 5b). These evidences agree with the microhardness values (Figure 5 and 6).

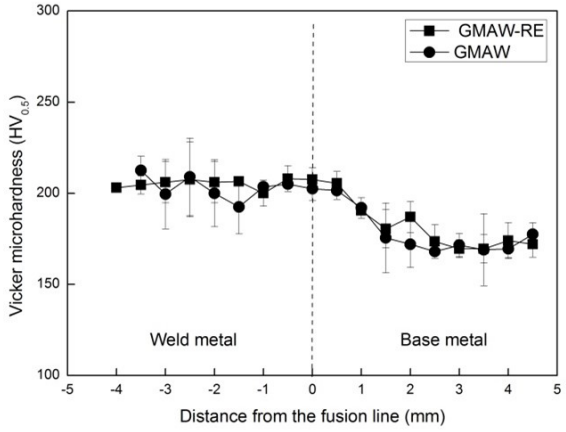

Figure 6. Microhardness profile obtained at different distances from the fusion line.

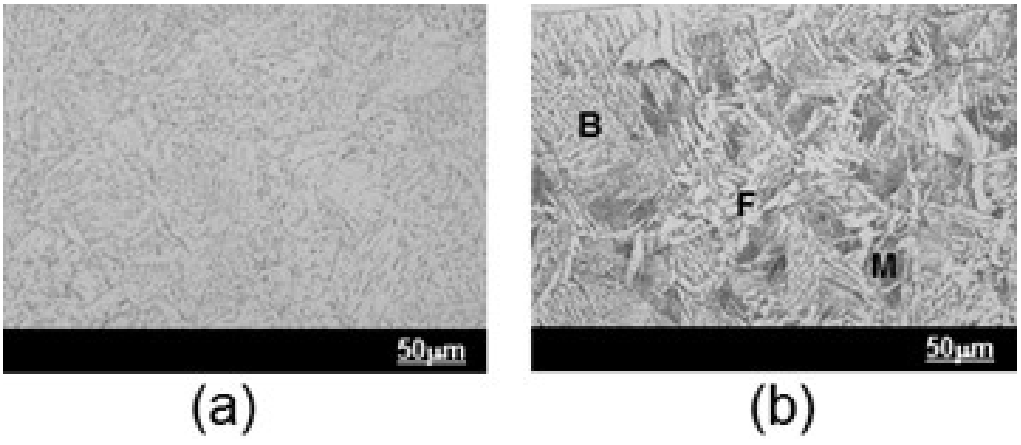

Figure 7. Microstructure of the CGHAZ after etching with 2% nital (OM). (a) GMAW-RE (206+/-6 $HV_{0.5}$); (b) GMAW (202+/-5 $HV_{0.5}$). (B)-bainite; (F) -ferrite and (M)-martensite.

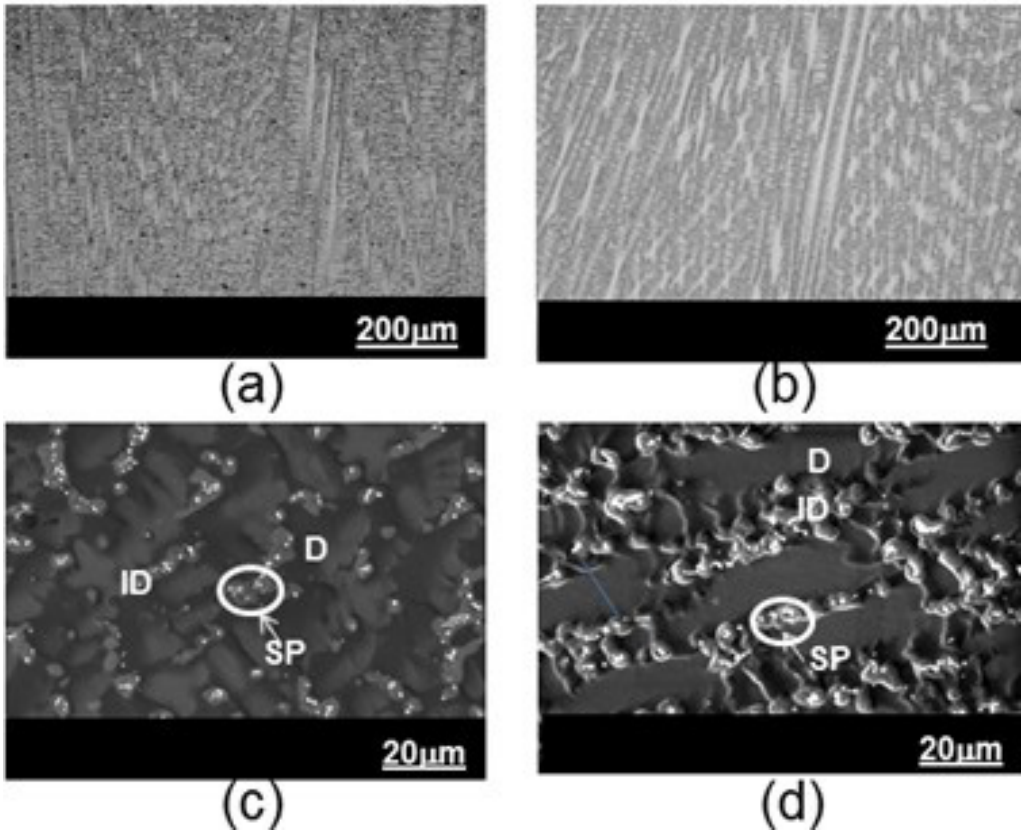

Figure 8. Microstructure of the deposited weld metals after etching with oxalic acid. (a) OM image - GMAW-RE; (b) OM image – GMAW; (c) SEM image - GMAW-RE; (d) SEM image - GMAW. SEM images were obtained in secondary electron mode. Where: D - Dendritic area, ID – Interdendritic area; SP – Secondary phase.

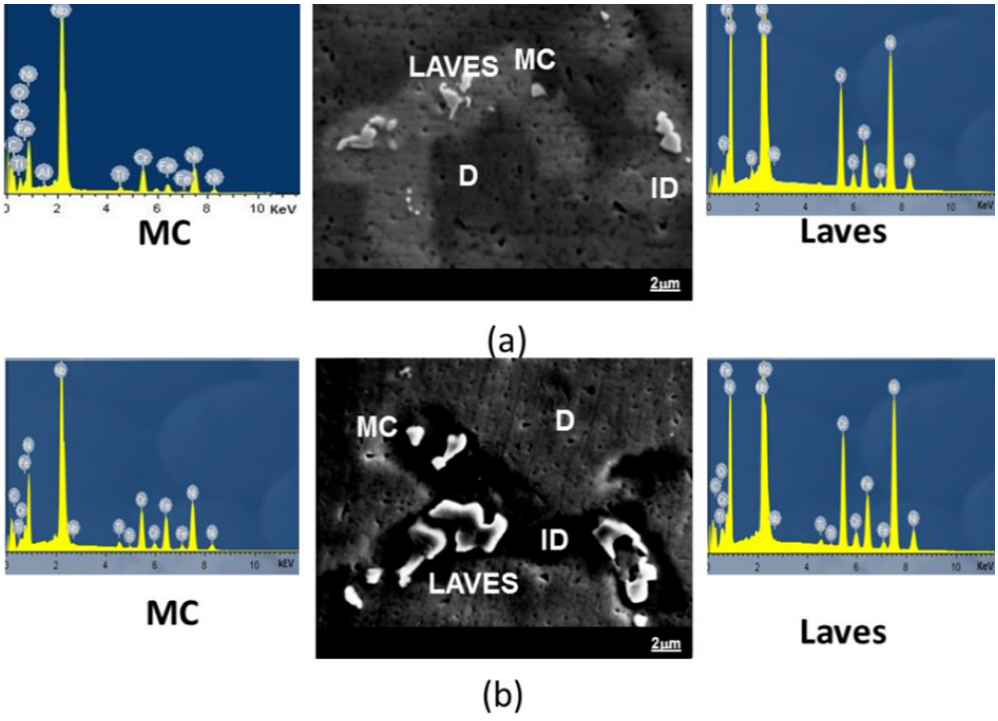

Figure 9. SEM images and EDS analysis of the microstructure of the weld metal after etching with oxalic acid. (a) GMAW-RE; (b) GMAW. Where: D - Dendritic Region, ID – Inter-dendritic Region, MC – Carbide.

According to DuPont et al. [42], although solid solute nickel-based alloys solidify as austenite (γ), alloying elements segregate during the solidification and secondary phases nucleate in the interdendritic areas, following Equation 2.

$$L \rightarrow L + \gamma \rightarrow L + \gamma + MC \rightarrow L + \gamma + MC + Laves \rightarrow \gamma + MC + Laves \quad (2)$$

The solidification of Inconel 625 initially starts with the nucleation of austenite and the solid/liquid interface sweeps out alloying elements such as niobium, titanium, and carbon into the liquid metal. As a consequence, MC-type carbides are formed via the eutectic reaction in the niobium, titanium, and carbon-rich solidification zone. Laves phase occurs together with MC-type carbides [40,42]. Although niobium is used for solid solution strengthening in Inconel 625, this element contributes strongly to the formation of MC-type carbides and Laves phases due to its higher segregation tendency. The results obtained in this work are in line with these statements. Table 4 shows that interdendritic areas are enriched with Mo and Nb, confirming the important effect of these elements on the formation of secondary phases shown in Figure 9.

From Tables 3 and 4, it is also important to emphasize the higher Fe content in GMAW weld metals. Similar values are observed in other works [11,12,51], regardless of the shielding gas applied. It is an expected result because an increase in dilution promotes an increase in Fe content [42]. Another consequence of the higher Fe content is the decrease of solubility of niobium and molybdenum, in turn increasing their segregation in the interdendritic phases and promoting a higher fraction of secondary phases [52], confirming this scenario. Different behavior is provided by the GMAW-RE process, where the Fe content is close to the value required even for a single layer. Although no result reports involving specifically the GMAW-RE are available, it is believed that it is an expected behavior because the rotation of the arc provides a better distribution of the heating, as observed when the weaving technique was compared to the stringer deposit [53,54].

Although the global dilution rate calculated from the area of base metal related to the total area of weld metal is widely adopted as a parameter to support the results, there are applications where the local dilution is more suitable. Particularly in the oil and gas industry, a maximum Fe content at the finished surface of 10% [8] for optimum pitting corrosion resistance is a parameter applied to characterize the quality of the overlay. It is noted that the results of local dilution are higher than those predicted by global dilution, indicating that the calculation of dilution following the recommendation of the current standards regarding the maximum Fe content, seems to be most appropriate taking into account its more conservative aspect.

Based on the above discussion, it is believed that the GMAW-RE process has the potential to produce weld overlays with adequate quality. As the thickness of the single layer is almost suitable, it is suggested that a single layer with acceptable performance can be obtained with adjustments in the main operational parameters, hence reducing the costs. As observed in other works [7,13,19], the optimization of parameters, such as welding current, welding speed, angle torch, preheat, track overlap, and arc oscillation can improve the results by reducing the dilution ratio. Particularly for the GMAW-RE process, adjusts in rotation frequency and rotation diameter can offer additional alternatives for superior results, mainly the reduction of the Fe content, thus achieving acceptable mechanical and corrosion properties in single layer claddings, as observed in a recent work [55].

Although the literature reports that other processes can provide lower dilution ratios than the values obtained in this work, the GMAW-RE could attain the acceptable thickness with a lower volume of deposited weld metal, indicating a better overall performance.

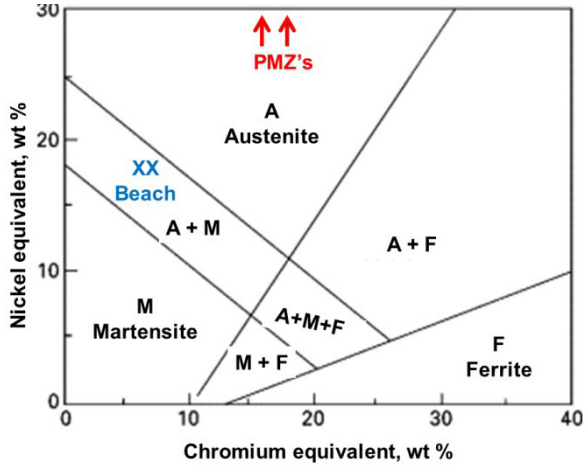

Figure 10. Schaeffler diagram indicating the microstructure of the PMZs and beach discontinuity.

Table 4. The elemental composition range of the regions at the top of the weld deposits was obtained by the SEM/EDS point microanalysis

Weld metal	Position	Cr	Ni	Fe	Mo	Nb
GMAW-RE	Matrix (ID)	18.2	52.3	12.6	10.5	6.5
	Matrix (D)	19.3	56.0	14.7	7.9	2.1
GMAW	Matrix (ID)	16.2	47.5	21.9	9.1	4.7
	Matrix (D)	17.1	49.6	24.7	7.1	1.6

Where: D dendritic, ID interdendritic.

The present results encourage future works addressing the GMAW-RE process as an alternative solution to produce claddings for the industry.

5 Conclusions

The following main conclusions can be drawn from the presented analysis:

(a) Weld overlay claddings deposited by the GMAW-RE process show a more homogeneous bead profile, higher thickness, and lower dilution ratio compared to the GMAW process;

(b) The weld metal deposited by the GMAW-RE shows an austenitic matrix with a reduced fraction of secondary phases compared with the GMAW process;

(c) The GMAW-RE process shows the potential to be a cost-effective alternative to claddings because a suitable single-layer weld overlay cladding is expected with optimized welding parameters.

Acknowledgments

The authors would like to acknowledge CEFET-RJ and WHITE MARTINS for their support in the execution of the present work.

References

1 He K, Dong L, Wang Q, Zhang H, Li Y, Liu L, et al. Comparison on the microstructure and corrosion behavior of Inconel 625 cladding deposited by tungsten inert gas and cold metal transfer process. Surface and Coatings Technology. 2022;435:128245. http://doi.org/10.1016/j.surfcoat.2022.128245.

2 Evangeline A, Sathiya P. Dissimilar cladding of Ni–Cr–Mo super alloy over 316L austenitic stainless steel: morphologies and mechanical properties. Metals and Materials International. 2021;27:1155-1172. http://doi.org/10.1007/s12540-019-00440-x.

3 Singhal TS, Jain JK. GMAW cladding on metals to impart anti-corrosiveness: machine, processes, and materials. Materials Today: Proceedings. 2020;26(2):2432-2441. http://doi.org/10.1016/j.matpr.2020.02.518.

4 Moura BB, Souza D, Silva MO, Osorio AG. Effect of inert and active shielding gases in the corrosion resistance of IN 625 weld overlays. Journal of Materials Engineering and Performance. 2022;31:5886-5897. http://doi.org/10.1007/s11665-022-06651-5.

5 Mota CAM, Nascimento AS, Garcia DN, Silva DAS, Teixeira FR, Ferraresi VA. Nickel overlay deposited by MIG welding and cold wire MIG welding. Weld Int. 2018;32(9):588-598. http://doi.org/10.1080/09507116.2017.1347333.

6 Elango P, Balaguru S. Welding parameters for Inconel 625 overlay on carbon steel using GMAW. Indian Journal of Science and Technology. 2015;8(31):1-5.

7 Tabaie S, Greene T, Benoit MJ. Optimization of GMAW process parameters for weld overlay of Inconel 686 superalloy on low-carbon steel. International Journal of Advanced Manufacturing Technology. 2023;127:4769-4788. http://doi.org/10.1007/s00170-023-11798-z.

8 Norsok Standard. M-001, Materials selection. Oslo, Norway: Norsok Standard; 2004.

9 Petrobras. Technical Specification, Welding, I-ET-3010.00-1200-955-P4X-001. Petrobras; 2020. 74 p.

10 Araujo FPD, Mainier FB, Almeida BB. Evaluation of Ni-Cr-Mo alloy applied by weld overlay cladding on carbon steel for use in NaCl 3.5% mass solution. Proc. on Eng Sci. 2021;3(3):355-364. http://doi.org/10.24874/PES03.03.011.

11 Mougo AL, Bentes Neto FMA, Garcia DN, Mota CAM. Effect of a cold wire on the metallurgical characteristics of nickel-based welds deposited by GMAW-CW. Transactions of the Indian Institute of Metals. 2020;73:2425-2434. http://doi.org/10.1007/s12666-020-02068-7.

12 Posch G, Scherleitner W, Rutzinger B, Schmitt G, Kamath V, Fiedler M. Manufacturing of nickel base-overlays: comparison of various welding Technologies under consideration of clad properties. In: Proceedings of the IIW International Congress IC 2014; 2014; New Delhi, India. New Delhi: International Institute of Welding; 2014. p. 1-8.

13 Volpi A, Serra G. Weld overlay of highly corrosion resistant nickel, chromium, molybdenum alloys UNS N06059 on low alloy equipment operating at high temperature. In: Proceedings of the ASME 2018 symposium on elevated temperature application of materials for fossil, nuclear, and petrochemical industries ETAM; 2018 April 3-5; Seattle, WA, USA. USA: ASME; 2018. 12 p. Paper ETAM2018-6715, V001T02A003. https://doi.org/10.1115/ETAM2018-6715.

14 Rozmus-Górnikowska M, Kusiński J, Cempura G, Morgiel J. Microstructure and phase composition of transition zone between low alloyed steel boiler tube and an austenitic stainless steel weld overlay produced by cold metal transfer method. International Journal of Pressure Vessels and Piping. 2023:104951. https://doi.org/10.1016/j.ijpvp.2023.104951.

15 Babyak T, DeCenso V, Alexandrov B, Penso J. Application of low heat input gas metal arc welding for corrosion resistant weld overlays. Proc. of the ASME 2020 Pressure Vessels & Piping Conference, PVP2020; 2020 July 19-24;, USA. USA:American Society of Mechanical Engineers; 2020. p. 1-7. Paper PVP2020-21562.

16 Alvarães CP, Jorge JCF, Souza LFG, Araújo LS, Mendes MC, Farneze HN. Microstructure and corrosion properties of single layer Inconel 625 weld cladding obtained by the electroslag welding process. Journal of Materials Research and Technology. 2020;9(6):16146-16158. http://doi.org/10.1016/j.jmrt.2020.11.048.

17 Alvaraes CP, Sandes SS, Jorge JCF, Souza LFG, Araujo Mendes MC, Dille J. Microstructural characterization of Inconel 625 nickel-based alloy weld cladding obtained by electroslag welding process. Journal of Materials Engineering and Performance. 2020;29:3004-3015. http://doi.org/10.1007/s11665-020-04861-3.

18 Azevedo RO Jr, Costa JFM, Magalhães HAY, Jorge JCF, de Souza LFG, Mendes MC, et al. GMAW process with rotating electrode: an advanced alternative to improve cladding performance. Journal of Adhesion Science and Technology. 2023;38(10):1782-1793. http://doi.org/10.1080/01694243.2023.2270179.

19 Evangeline A, Sathyia P. Structure-property relationships of Inconel 625 cladding on AISI 316L substrate produced by hot wire (HW) TIG metal deposition technique. Materials Research Express. 2019;6:106539. http://doi.org/10.1088/2053-1591/ab350f.

20 Knerek R, Lemos GVB, Vander Voort G, Freitas DA, Haupt W, Landell R, Buzzatti D. Investigating an API X65 steel pipe cladded with alloy 625. Tecnolologia em Metalurgia, Materiais e Mineração. 2021;18:e2465. http://doi.org/10.4322/2176-1523.20212465.

21 Beaugrand VCM, Smith LS, Gittos MF. Hydrogen embrittlement of 8630M/625 subsea dissimilar joints: factors that influence the performance. In: Proceedings of the 22nd International Conference on Ocean, Offshore and Arctic Engineering; 2009 May 29-June 5, Honolulu, Hawaii. Honolulu: American Society of Mechanical Engineers; 2009. p. 1-10. Paper OMAE 2009-8003.

22 Beaugrand VCM, Gittos MF. Subsea dissimilar joints: failure mechanisms and opportunities for mitigation. In: Corrosion, 2009 March 22-26; Atlanta, Georgia, USA. Atlanta: The Welding Institute; 2009. p. 1-11. Paper 09305.

23 Farias FWC. Payão Fo JC, Azevedo LMB. Microstructural and mechanical characterization of the transition zone of 9%Ni steel cladded with Ni-based superalloy 625 by GTAW-HW. Metals. 2018;8(12):1007. https://doi.org/10.3390/met8121007.

24 Monine VI, Gonzaga RS, Farias FWC, Passos EKD, Payão Fo JC. Study of mechanical behavior and X-ray elastic constants of nickel alloy weld overlay. Materials Research. 2019;22(4):e20180719. http://doi.org/10.1590/1980-5373-MR-2018-0719.

25 Guo L, Zheng H, Liu S, Li Y, Xu X, Feng C. Formation quality optimization and corrosion performance of Inconel 625 weld overlay using hot wire pulsed TIG rare metal. Materials & Design. 2016;45(9):2219-2226.

26 Najafi M, Bakhshayesh MM, Farzadi A. Microstructure and phase analysis of multilayer Ni–Cr–Mo clad for corrosion protection. Transactions of the Indian Institute of Metals. 2021;74:1663-1672. http://doi.org/10.1007/s12666-021-02256-z.

27 Xu L, Shao C, Tian L, Zhang J, Han Y, Zhao L, et al. Intergranular corrosion behavior of Inconel 625 deposited by CMT/GTAW. Corrosion Science. 2022;201:110295. http://doi.org/10.1016/j.corsci.2022.110295.

28 Guo L, Xiao F, Wang F, He Y, Wei W, Zhang Y. Microstructure and corrosion resistance of Inconel 625 overlay welded by pulsed TIG process. International Journal of Electrochemical Science. 2021;16:210418. http://doi.org/10.20964/2021.04.11.

29 Silveira GMS, Silva WA Fo, Costa JFM, Mendes MC, Souza LFG, Jorge JCF. Influence of rotation frequency and rotation diameter on Mechanical properties and microstructure of weld metal produced by MCAW-RE. International Journal of Advanced Manufacturing Technology. 2020;110:1789-1803. http://doi.org/10.1007/s00170-020-05961-z.

30 Sankar N, Malarvizhi S, Balasubramanian V, Hafeezur Rahman A, Balaguru V. Effect of rotating arc (Spin Arc) on mechanical properties and microstructural characteristics of gas metal arc welded armour steel joints. Transactions of the Indian Institute of Metals. 2022;75:3047-3059. http://doi.org/10.1007/s12666-022-02679-2.

31 Silva WA Fo, Silveira GMS, Costa JFM, Mendes MC, Souza LFG, Jorge JCF. Microstructure and impact toughness of high strength steel weld metals deposited by MCAW-RE process using different shielding gases. International Journal of Advanced Manufacturing Technology. 2021;115:3105-3120. http://doi.org/10.1007/s00170-021-07353-3.

32 American Welding Society. AWS A5.14/A5.14M:2005, Specification for nickel and nickel-Alloy bare welding electrodes and rods. Miami: American Welding Society; 2005.

33 American Society for Testing Materials. ASTM E384-17, Standard test method for microindentation hardness of materials. West Conshohocken: ASTM International; 2017

34 Jorge JCF, Meira OG, Madalena FCA, Souza LFG, Araújo LS, Mendes MC. Evaluation of the AISI 904L alloy weld overlays obtained by GMAW and electro-slag welding processes. Journal of Materials Engineering and Performance. 2017;26(5):2204-2212. http://doi.org/10.1007/s11665-017-2631-9.

35 Najafi M, Bakhshayesh MM, Farzadi A. Microstructure and phase analysis of multilayer Ni–Cr–Mo clad for corrosion protection. Transactions of the Indian Institute of Metals. 2021;74:1663-1672. http://doi.org/10.1007/s12666-021-02256-z.

36 Souza D, Tavares AF, Costa HL, Osorio AG. Efeito da energia de soldagem sobre a microestrutura e resistência à corrosão de revestimentos de Inconel 625 aplicados pelo processo GMAW. Matéria (Rio de Janeiro). 2020;25(2):1-17. http://doi.org/10.1590/S1517-707620200002.1033.

37 Akselsen OM, Bjørge R, Ånes HW, Ren X, Nyhus B. Microstructure and properties of wire arc additive manufacturing of Inconel 625. Metals. 2022;12:1867. http://doi.org/10.3390/ met12111867.

38 Zhang C, Qiu Z, Zhu H, Wang Z, Muránsky O, Ionescu M, et al. On the effect of heat input and interpass temperature on the performance of Inconel 625 alloy deposited using wire arc additive manufacturing - cold metal transfer process. Metals. 2022;12:46. http://doi.org/10.3390/met12010046.

39 Frei J, Alexandrov BT, Rethmeier M. Low heat input gas metal arc welding for dissimilar metal weld overlays part II: the transition zone. Welding in the World. 2018;62:317-324. http://doi.org/10.1007/s40194-017-0539-5.

40 Silva CC, Miranda HC, Motta MF, Farias JP, Afonso CRM, Ramirez AJ. New insight on the solidification path of an alloy 625 weld overlay. Journal of Materials Research and Technology. 2013;2(3):228-237. http://doi.org/10.1016/j.jmrt.2013.02.008.

41 Alvarães CP, Madalen FCA, Souza LFG, Jorge JCF, Araújo LS, Mendes MC. Performance of the Inconel 625 weld overlay obtained by FCAW process. Matéria (Rio de Janeiro). 2019;24(1):e12290. http://doi.org/10.1590/S1517-707620190001.0627.

42 DuPont JN, Lippold JC, Kiser SD. Welding metallurgy and weldability of nickel-base alloys. New Jersey: Wiley; 2009.

43 Banovic SW, DuPont JN, Marder AR. Dilution and microsegregation in dissimilar metal welds between super austenitic stainless steel and nickel base alloys. Science and Technology of Welding and Joining. 2002;7:374-383. http://doi.org/10.1179/136217102225006804.

44 Zhang H, Chang Q, Liu J, Lu H, Wu H, Feng J. A novel rotating wire GMAW process to change fusion zone shape and microstructure of mild steel. Materials Letters. 2014;123:101-103. https://doi.org/10.1016/j.matlet.2014.03.018 .

45 Bai Q, Guo N, Han Y, Zhang J, Wang M. Analysis of temperature distribution in rotating arc welding. Advanced Materials Research. 2012;472-475:1346-1352. http://doi.org/10.4028/www.scientific.net/AMR.472-475.1346.

46 Silva RHG, Schwedersky MB, Santos AGM, Okuyama MP. Effects of the rotating arc technique on the GMA welding process. Soldagem e Inspeção. 2020;25:e2519. http://doi.org/10.1590/0104-9224/SI25.19.

47 Srinivasa Rao P, Gupta OP, Murty SSN. A study on the weld bead characteristics in pulsed gas metal arc welding with rotating arc. In: Proceedings of the of 23rd International Conference on Offshore Mechanics and Arctic Engineering; 2004 June 20-25; Vancouver, Canada. Vancouver: American Society of Mechanical Engineers; 2004. p. 1-5. Paper OMAE2004-51580.

48 Yang YK, Kou S. Fusion-boundary macrosegregation in dissimilar-filler welds. Welding Journal. 2007;86:303-312.

49 Kejelin NZ, Buschinelli AJA, Pope AM. Effect of welding parameters on the partially diluted zones formation at dissimilar metal welds. In:Proceedings of the 18th International Congress of Mechanical Engineering; 2005; Ouro Preto, Brazil. Ouro Preto: Brazilian Association of Engineering and Mechanical Science; 2005. p. 1-8.

50 Dai T, Lippold JC. Tempering effect on the fusion boundary region of alloy 625 weld overlay on 8630 steel. Welding in the World. 2018;62:535-550. http://doi.org/10.1007/s40194-018-0560-3.

51 Rutzinger B. Influence of the welding process to the dilution rate of weld overlays on unalloyed steel using the weld consumable ERNiCrMo-3 (Alloy 625). BiulInstSpawalnictwa. 2014;5:72-75.

52 Lorenzoni RA, Gasparini RP, Santos AC, Luz TS, Macêdo MCS. A study on the intergranular corrosion and pitting resistance of Inconel 625 coating by PTA-P. Corrosion Engineering, Science and Technology. 2019;54(1):62-74. http://doi.org/10.1080/1478422X.2018.1533677.

53 Tasalloti H, Kah P, Martikainen J. Effects of welding wire and torch weaving on GMAW of S355MC and AISI 304L dissimilar welds. International Journal of Advanced Manufacturing Technology. 2014;71:197-205. http://doi.org/10.1007/s00170-013-5484-x.

54 Cavalcante NE, Andrade TC, Pinheiro PHM, Miranda HC, Motta MF, Aguiar WM. Study of MIG/MAG welding procedures for application of coatings of Inconel 625 nickel alloy on ASTM A387 Gr.11 structural steel. Welding International. 2018;32(2):112-121. http://doi.org/10.1080/09507116.2017.1347324.

55 Costa JFM, Lacerda PL, Magalhães HAY, Jorge JCF, Souza LFG, Mendes MC, et al. Inconel 625 weld claddings obtained by the GMAWRE with rotating Electrode. International Journal of Advanced Manufacturing Technology. 2024;132:5647-5661. http://doi.org/10.1007/s00170-024-13697-3.

Received: 3 Mar. 2023
Accepted: 15 May. 2024